

# The Ultraviolet Radiation Environment of a Tropical Megacity in Transition: Mexico City

## 2000-2019

Adriana Ipiña,<sup>\*,†,‡</sup> Gamaliel López-Padilla,<sup>¶</sup> Armando Retama,<sup>§</sup> Rubén D. Piacentini,<sup>†</sup> and Sasha Madronich<sup>||</sup>

<sup>†</sup>*Instituto de Física Rosario (CONICET-UNR), Rosario, Argentina*

<sup>‡</sup>*Centro de Ciencias de la Atmósfera, Universidad Nacional Autónoma de México, Mexico City, Mexico*

<sup>¶</sup>*Facultad de Ciencias Físico Matemáticas, Universidad Autónoma de Nuevo León, San Nicolás de los Garza, México*

<sup>§</sup>*Independent researcher, Mexico City, Mexico*

<sup>||</sup>*National Center for Atmospheric Research, Boulder, Colorado, USA*

E-mail: [ipina@ifir-conicet.gov.ar](mailto:ipina@ifir-conicet.gov.ar)

### Abstract

Tropical regions experience naturally high levels of UV radiation, but urban pollution can reduce these levels substantially. We analyzed 20 years of measurements of the UV Index (UVI) at several ground-level locations in the Mexico City Metropolitan Area and compared these with UVI values estimated from satellite overpasses observing ozone and clouds (but not local pollution). The ground-based measurements were systematically lower than the satellite-based estimates, by ca. 40% in 2000 and 20% in 2019. Calculations with a radiative transfer model and observed concentrations of air

9 pollutants explained well the difference between satellite- and ground-based UVI, and  
10 showed specific contributions from boundary layer and free tropospheric aerosols, O<sub>3</sub>,  
11 NO<sub>2</sub>, and SO<sub>2</sub>, in decreasing order of importance. Such large changes in UV radiation  
12 between 2000 and 2019 have important implications ranging from human health (skin  
13 cancer and cataract induction) to air pollution control (photochemical smog formation).

## 14 Introduction

15 Ultraviolet (UV) radiation is an important component of the urban environment, affecting  
16 human populations directly through UV exposure of skin and eyes<sup>1–3</sup> and less directly (but  
17 with great impact) by driving the formation of photochemical smog, including tropospheric  
18 ozone and other oxidants, as well as secondary aerosols containing nitrates, sulfates, and  
19 organics.<sup>4–6</sup> These pollutants, along with others of primary origin commonly found in ur-  
20 ban atmospheres (e.g., black carbon, sulfur dioxide), can in turn scatter and/or absorb UV  
21 radiation, alter its vertical distribution, and so modify the photochemical rate of their own  
22 formation. Such feedback complicates the calculation of both the UV radiation field (in-  
23 cluding at the surface), and the evolution of photochemical smog in the urban boundary  
24 layer.

25 The question of how air pollution alters the urban UV environment (and *vice versa*) is  
26 not new, but studies have relied mostly on numerical models,<sup>7–9</sup> with relatively fewer avail-  
27 able observations (e.g., McKenzie et al.<sup>10</sup>, Panicker et al.<sup>11</sup>, Palancar et al.<sup>12</sup>, reviewed by  
28 Bais et al.<sup>13</sup>). Increases in UV have been estimated in association with decadal emission  
29 reductions, e.g. in China,<sup>14–16</sup> and that have led to less-than-expected reductions in photo-  
30 chemical smog, in part due to stronger UV photochemistry.<sup>17? ,18</sup> Emission reductions have  
31 also occurred globally during the 2020 COVID-19 pandemic,<sup>19,20</sup> but ground-level ozone in  
32 some polluted areas has actually increased,<sup>21,22</sup> due at least in part to the increased UV ra-  
33 diation. Unfortunately, the observational data base of relevant UV radiation remains rather  
34 sparse to evaluate such model-derived hypotheses.

35       The environment of Mexico City is of particular interest for several reasons: (1) Nearly  
36      23 million people inhabit the Mexico City Metropolitan Area (MCMA), and the UV environ-  
37      ment has direct implications for their health, both in terms of skin/eye UV exposure and *via*  
38      photochemical smog formation. (2) As a tropical megacity, it is to some extent representative  
39      of the situation of many others, with year-round intense midday UV irradiance, a shallower  
40      atmosphere due to the city's high elevation of 2240 m above sea level, and a transition to-  
41      ward newer and cleaner technologies, leading to gradual improvements in air quality. (3) Air  
42      quality within MCMA has undergone extensive scrutiny, with a well-established monitoring  
43      network since 1986,<sup>23</sup> numerous intensive field campaigns to study the meteorology, emis-  
44      sions, and photochemistry of smog formation,<sup>24–26</sup> and numerical modeling incorporating  
45      the evolving knowledge.<sup>27–30</sup> This extensive body of knowledge provides the foundation for  
46      understanding our study.

47       Here, we analyze two decades of continuous measurements of the UV Index at multiple  
48      locations within the MCMA, collected by the Secretariat of the Environment (Secretaría  
49      del Medio Ambiente, SEDEMA)<sup>1</sup> of the Mexico City government as part of an intensive  
50      monitoring network over the MCMA. The UV Index is defined as:

$$UVI = 40 \int_{250nm}^{400nm} E(\lambda, t) \cdot S_{er}(\lambda) d\lambda \quad (1)$$

51       where  $E(\lambda, t)$  is the solar spectral irradiance in units of  $\text{W} \cdot \text{m}^{-2} \cdot \text{nm}^{-1}$  and  $S_{er}(\lambda)$  is  
52      the erythemal sensitivity of human skin.<sup>31,32</sup> Multiplication by 40 was chosen historically to  
53      express the UVI in small integer numbers, but is otherwise scientifically arbitrary.

54       The UVI is recognized by the World Health and Meteorological Organizations (WHO  
55      and WMO) as a standardized metric of UV radiation<sup>31</sup> for global public information. An  
56      advantage of using the UVI as (one) metric of UV radiation is that it is being increasingly  
57      observed or calculated and disseminated, enabling more objective comparisons among seasons  
58      and locations. The UVI observations from Mexico City, considered here, are an important

---

<sup>1</sup><https://www.sedema.cdmx.gob.mx/>

59 element of this global picture.

60 While the UVI at the surface cannot be translated directly into photolysis frequencies  
61 for various photo-labile molecules, the spectral weighting of the UVI (ca. 300-320 nm) is  
62 approximately similar to that for the photolysis of ozone to singlet oxygen atoms. Other UV  
63 wavelengths are of course also important, e.g. for the photolysis of nitrogen dioxide, and  
64 may be affected differently depending on the pollutant. With these considerations and a few  
65 other caveats, UVI trends examined here can also be used to infer accompanying trends in  
66 photolysis frequencies and influences on photochemical smog formation.

## 67 Methods

### 68 Ground-based measurements

69 The Mexico City Metropolitan Area is located at 19.4°N, 99.1°W, 2240 meters above sea  
70 level (asl), surrounded by mountain ridges exceeding 5000 m asl, with complex topography  
71 and thermal inversions that inhibit winds and favor intense air pollution.<sup>33-35</sup> Air quality  
72 monitoring and surface meteorological measurements in the MCMA are conducted continu-  
73 ously by the Automated Atmospheric Monitoring Network (RAMA, by its Spanish acronym)  
74 of the Atmospheric Monitoring System (SIMAT, by its Spanish acronym) of the Mexico City  
75 government. Since the year 2000, UV radiometers (model 501-A, Solar Light Company Inc.,  
76 Glenside, PA) detecting wavelengths between 280-400 nm have been measuring erythemally-  
77 weighted solar radiation. The calibration of the UV sensors was carried out annually by  
78 comparing against a factory-calibrated reference sensor. The output voltages from the mea-  
79 suring sensors were compared during at least one week against the UV readings from the  
80 reference sensor to derive the calibration factor. New calibration factors typically differed  
81 from the old ones by 2% or less. Reference sensors were also calibrated by the manufacturer  
82 and updated periodically (between 3 to 5 years) to avoid any bias due to aging. Long term  
83 calibration drift was avoided by the yearly re-calibrations. Although at the beginning only

84 a few stations were in operation and have been changing, currently 11 stations are record-  
 85 ing erythemal irradiances, which are then multiplied by 40 (see Eq. 1) to give UV Indices.  
 86 Table 1 describes the location of the stations where UV Index has been measured. Figure 1  
 87 shows how the radiometers of the SIMAT have been distributed over MCMA, prioritizing  
 88 the sites with more density of population. Near real-time data for each station are available  
 89 on the SIMAT official website <http://www.aire.cdmx.gob.mx/default.php>. Daily maxi-  
 90 mum values ( $UVI_{max}$ ) were extracted from each of the stations around solar noon from the  
 91 time interval from 11:00 h-15:00 h CST (Central Standard Time). This database with 7305  
 92 continuous days of measurements during the period 2000-2019 was analyzed.

Table 1: SIMAT stations and AERONET site\*, environmental descriptors and geographical positions. Abbreviations names: Chalco (CHA), Cuautitlán (CUT), FES Acatlán (FAC), Hangares (HAN), Laboratorio de Análisis Ambiental (LAA), Merced (MER), Montecillo (MON), Milpa Alta (MPA), Pedregal (PED), San Agustín (SAG), Santa Fe (SFE), Tlalnepantla (TLA) and National Autonomous University of Mexico (UNAM\*)

Station	Environment	Lat (°N)	Lon (°W)	El (masl)
CHO	semi-urban	19.27	98.89	2253
CUT	ecological park	19.72	99.20	2263
FAC	urban	19.48	99.24	2299
HAN	urban	19.42	99.08	2235
LAA	urban	19.48	99.15	2255
MER	downtown	19.42	99.12	2245
MON	rural	19.46	98.90	2252
MPA	rural	19.18	98.99	2594
PED	residential	19.33	99.20	2326
SAG	urban	19.53	99.03	2241
SFE	residential	19.36	99.26	2599
TLA	urban	19.53	99.20	2311
UNAM*	University city	19.33	99.18	2294

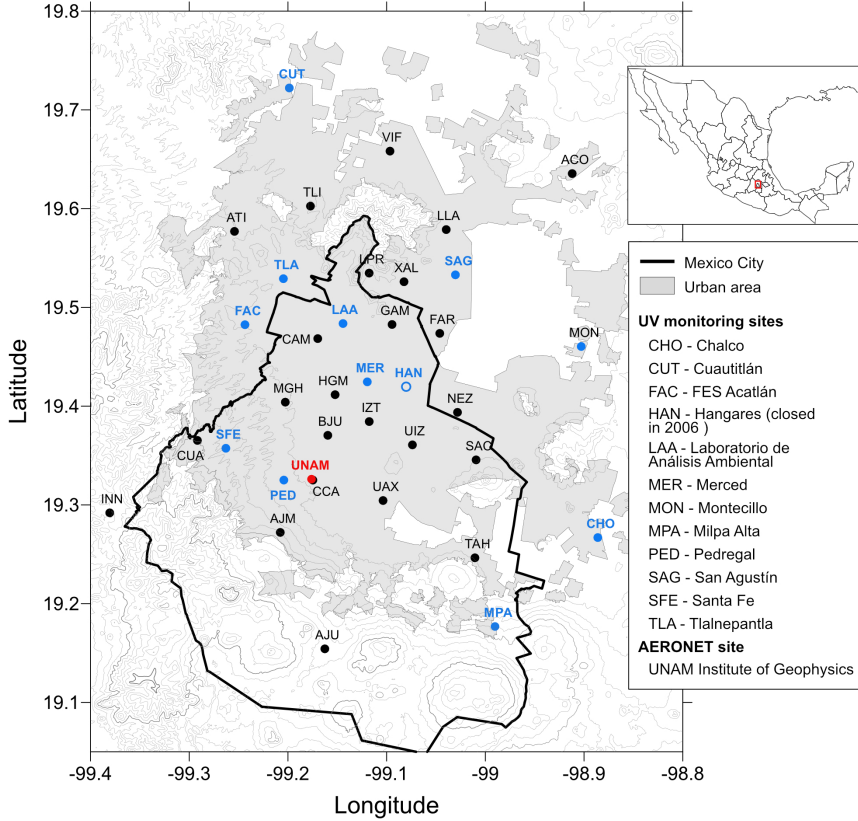


Figure 1: Map with the location of the SIMAT continuous monitoring stations over MCMA. Sites denoted by the blue solid dots correspond to SIMAT stations with UV measurements, while the black dots indicate SIMAT stations without UV measurements, the site on open blue dot represents a discontinued site, the red dot corresponds to the location of the AERONET site. The location of Mexico City and the acronyms of the UV and AERONET site are shown at the upper and lower frames at the right respectively.

With the aim to explore the relationship between UVI and air pollutants levels, the hourly averages for ozone ( $O_3$ ), carbon monoxide (CO), nitrogen dioxide ( $NO_2$ ), sulfur dioxide ( $SO_2$ ) and particle matter with diameter sizes  $\leq 10 \mu m$  ( $PM_{10}$ ), were downloaded from the SIMAT.<sup>36</sup> For purposes of assessing the influence on the UV Index at solar noon, only values obtained between 11h and 15h CST were considered for the trends analysis. Pollutant measurements are conducted by the SIMAT using regulatory-grade commercial instruments. Measurement principles include ultraviolet photometry (model 400E, Teledyne-API) for  $O_3$ , chemiluminescence (model 200E, Teledyne-API) for  $NO_2$ , UV fluorescence (model 100E, Teledyne API) for  $SO_2$ , and infrared absorption (model 300E, Teledyne-API) for CO.

<sup>102</sup> The PM<sub>10</sub> continuous mass concentration was measured with Tapered Element Oscillating  
<sup>103</sup> Microbalance (TEOM 1400AB or TEOM 1405 DF, Thermo Scientific) monitors. Gaseous  
<sup>104</sup> pollutant levels are reported in ppb concentration units for O<sub>3</sub>, SO<sub>2</sub> and NO<sub>2</sub>, and in ppm  
<sup>105</sup> for CO. Particulate matter mass concentration is reported in  $\mu\text{g m}^{-3}$  at local conditions for  
<sup>106</sup> temperature and pressure.

<sup>107</sup> Aerosol optical depth at 340 nm was obtained from the Institute of Geophysics of the  
<sup>108</sup> National Autonomous University of Mexico (UNAM); measurements were conducted with  
<sup>109</sup> a CIMEL sun photometer model CE-318, which is an automatic sun-sky-scanning spectral  
<sup>110</sup> radiometer of the AErosol RObotic NETwork (AERONET<sup>37</sup>). The data Product Level 2.0  
<sup>111</sup> and 1.5 (only in 2019) were selected, and annual averages AOD<sub>340</sub> were calculated along the  
<sup>112</sup> period 2000-2019, except for the year 2011 due to there were no measurements. A previous  
<sup>113</sup> study of the AOD behavior from 2000 to 2014 demonstrated that the gaps of data did not  
<sup>114</sup> significantly change the trends over the analyzed period.<sup>38</sup> From 2014 to 2019 there was only  
<sup>115</sup> 8% of the missing data, when the instrument was sent for calibration in 2018.

## <sup>116</sup> Satellite data

<sup>117</sup> The UV Index data derived from satellite measurements of reflected radiance were used for  
<sup>118</sup> comparing to the ground-based measurements. These data were provided by the Ozone  
<sup>119</sup> Monitoring Instrument (OMI) on board of AURA-NASA satellite.<sup>39</sup> OMI was created in co-  
<sup>120</sup> operation between the Netherlands Agency for Aerospace Programmes (NIVR), the Finnish  
<sup>121</sup> Meteorological Institute (FMI) and NASA. OMI (hereafter OMI-Aura/NIVR-FMI-NASA)  
<sup>122</sup> performs observations over a geographical dimension of 13×24km<sup>2</sup> at nadir. For the coor-  
<sup>123</sup> dinates (19.33N, 99.18W) and elevation (2268 masl) of Mexico City, the satellite overpass  
<sup>124</sup> time is between 19:00h - 21:00h UTC (20:00h - 22:00h CET). Measurements of the ozone  
<sup>125</sup> profile and cloud cover are used via a radiative transfer model to estimate the UVI at the  
<sup>126</sup> ground. The OMI web site reports UVI values for both the overpass time, and corrected to  
<sup>127</sup> local solar noon.

<sup>128</sup> While the early OMI estimates of the UVI did not account for the boundary layer aerosol  
<sup>129</sup> absorption, Arola et al.<sup>40</sup> proposed a postcorrection for absorbing aerosols based on global  
<sup>130</sup> monthly aerosol climatology. For Mexico City a reduction of about 8% is applied, starting  
<sup>131</sup> ca. 2013, to the OMI UVI data.

## <sup>132</sup> TUV model

<sup>133</sup> Calculations of the UV Index were also made with the Tropospheric Ultraviolet Visible  
<sup>134</sup> (TUV v5.3) model.<sup>41</sup> The model atmosphere was represented by 80 vertical layers, each 1  
<sup>135</sup> km thick, starting at the 2.24 km asl elevation of MCMA, and for which the first three km  
<sup>136</sup> constitute the atmospheric boundary layer (BL).<sup>42</sup> The ozone profile above the BL is from  
<sup>137</sup> the US Standard Atmosphere, but rescaled to a value of 259.6 DU. Totals including the BL  
<sup>138</sup> contributions (of 13.7 DU in the year 2000 and 9.8 DU in 2019, see below) were 273.1 DU  
<sup>139</sup> in 2000 and 269.2 DU. The climatological O<sub>3</sub> column for this latitude and season is about  
<sup>140</sup> 270 DU (plus or minus ca. 5 DU) so in good agreement with the values used here.

<sup>141</sup> Pollutants within the BL (including O<sub>3</sub>) are assumed to be well mixed, in agreement with  
<sup>142</sup> observations from the MILAGRO field campaign that showed the disappearance of vertical  
<sup>143</sup> gradients in the profiles of gases<sup>43,44</sup> and aerosols<sup>45,46</sup> by late morning. The UV-absorbing  
<sup>144</sup> gases considered here are O<sub>3</sub>, NO<sub>2</sub>, and SO<sub>2</sub>, specified in ppb.

<sup>145</sup> BL aerosols are modeled by prescribing the AOD at 340 nm (from AERONET observa-  
<sup>146</sup> tions), scaled to other wavelengths inversely with wavelength (Angstrom coefficient = 1.0),  
<sup>147</sup> asymmetry factor of 0.7, and a single scattering albedo of 0.85 at UV wavelengths, following  
<sup>148</sup> the determinations made in Mexico City by Corr et al.<sup>47</sup> and Palancar et al.<sup>12</sup>.

<sup>149</sup> Above the atmospheric boundary layer, the model was taken to be free of aerosols, NO<sub>2</sub>,  
<sup>150</sup> or SO<sub>2</sub>. In one sensitivity study, a total AOD of 0.7 was redistributed placing 0.2 in the  
<sup>151</sup> free troposphere (decreasing vertically with an exponential scale height of 4 km, and 0.5  
<sup>152</sup> remaining in the BL). The calculated UVI differed by less than 1%. Thus, as long as the  
<sup>153</sup> total AOD is known, knowledge of the exact vertical aerosol profile is not critical towards

154 ground-level UVI – but would obviously affect the vertical structure of photolysis frequencies.

155 Radiative transfer calculations were carried out with the pseudo-spherical 4-stream op-  
156 tion, at 1 nm steps between 280 and 400 nm.

## 157 Results and Discussion

158 Figure 2 shows the diurnal variation of the UVI for several specific cloud-free days, for  
159 different seasons and several locations (CHO, MER, MON, PED, SAG, SFE and TLA).  
160 UV Index from TUV model was used as reference of the behavior under clear sky days.

161 According to the comparison of measurements minute by minute, the dates with prolonged  
162 fluctuations along the day were discarded. However, during the rainy period (from June  
163 to October) at least a brief clouds presence is common, as shown at CHO station around  
164 noon in 13 June 2017. Peak values range from 8 during autumn/winter to above 12 in  
165 spring/summer, in correspondence to the respective December and June solstices. Although  
166 the stations are all within a 25 km radius, substantial differences among them are notable.

167 Survey of the locations revealed that shadowing from nearby structures is not an issue. The  
168 good agreement in the morning, followed by more divergence in the afternoon, is consistent  
169 with the development of photo-chemical pollution hotspots during the day. Previous studies

170 (e.g., Castro et al.<sup>48</sup> and Palancar et al.<sup>12</sup>) have shown that surface UV radiation in Mexico

171 City is attenuated significantly by aerosols. The measurements shown in Fig. 2 are consistent  
172 with this increasing pollution during the course of the day, with highest aerosol loading (and  
173 highest variability) attained in the afternoon. Further support for the role of pollution in

174 suppressing the UVI comes from the observation made at the Santa Fe (SFE) site which in

175 Fig. 2 are seen to be systematically higher, e.g. by over 10% in autumn afternoons, compared  
176 to the other stations. The SFE station is displaced to the west from the majority of the  
177 other stations, and remains in the outskirts. This site is also approximately 300 m higher  
178 than Mexico City downtown, so that the cleaner atmosphere results from both vertical and

179 horizontal variations in pollution levels.<sup>49</sup> It is indeed expected to have higher values of the  
 180 UVI, in agreement with the observations.

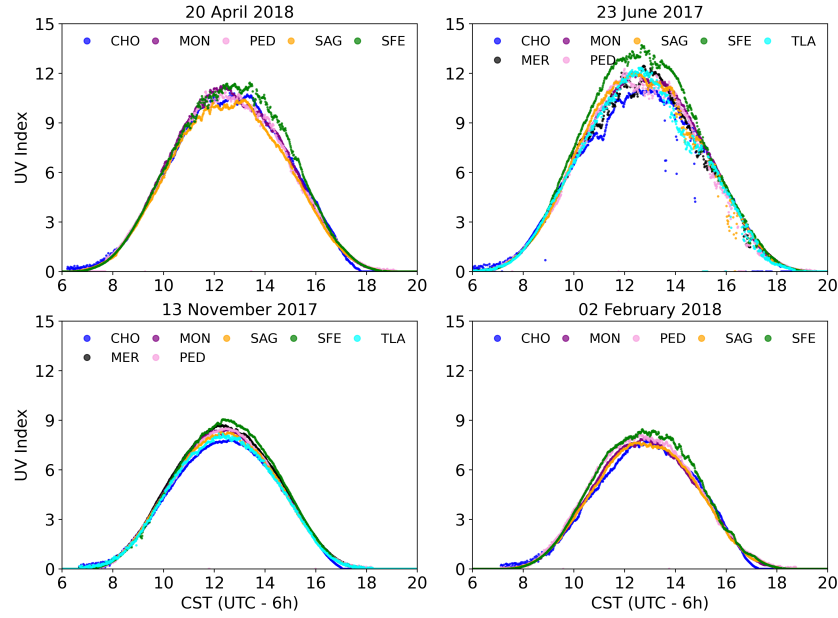


Figure 2: UV Index measured over MCMA by SIMAT stations each minute along the day under practically cloudless conditions for representative days of the year.

181 The daily maximum UV Index of each station is denoted by  $UVI_{max}$ , all of them were  
 182 counted in the period 2000-2019. As shown in Figure 3, these values ranged from 1 to  
 183 16, with a majority (61%) of the days experienced  $UVI_{max}$  values between 6 and 10, and  
 184 remarkably few, less than 1%, in the higher 13-16 range. The lowest values are likely due to  
 185 winter days with heavy cloud cover and low sun angles, and UV attenuation by pollutants  
 186 could also be amplified under such conditions, due to longer photon path lengths at low sun  
 187 and within clouds. The extreme sparsity of high UVI values remains surprising, and may be  
 188 an indication of the rarity of extremely unpolluted days within the city.

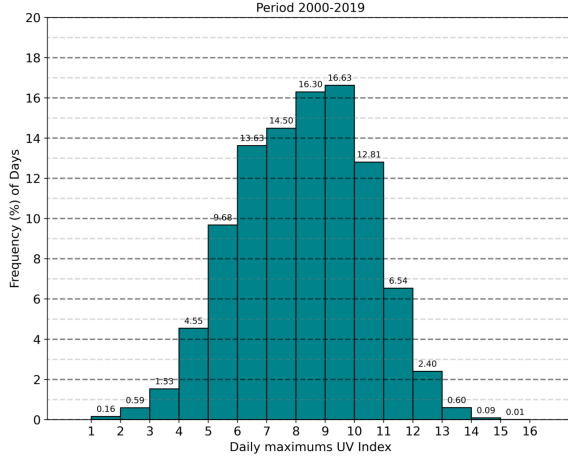


Figure 3: Frequency distribution of daily maximum UV Index values in Mexico City during 2000 -2019.

Similar patterns are found when considering the monthly average of the  $UVI_{\max}$  values as shown in Figure 4. The long-term averages present a seasonal variation (as in Fig. 2) that follows approximately the cosine of the noontime solar zenith angle. Notably, values rarely if ever exceed 12 (as in Fig. 3). The lowest average UVI (near 7) take place in winter while from March to August the values seem to be flattened in the range 10-11. The rather low monthly UV Index values, mainly could be a consequence of the presence of clouds in the rainy season. However, urban aerosol pollution sources, biomass burning for agriculture and wood cooking also contribute to poor air quality between March-May<sup>50</sup>. Using the maximum  $UVI_{\max}$  from all of stations every day (one daily point), the monthly averages ( $\overline{UVI}_m$ ) were calculated along the period 2000-2019 (except for June 2003 due to there were no measurements). Long term trends in  $\overline{UVI}_m$  are shown in Figure 5. A clear upward trend is seen, with a slope for the linear fit of 0.9%/year or +1.5 UVI units over the two decades.

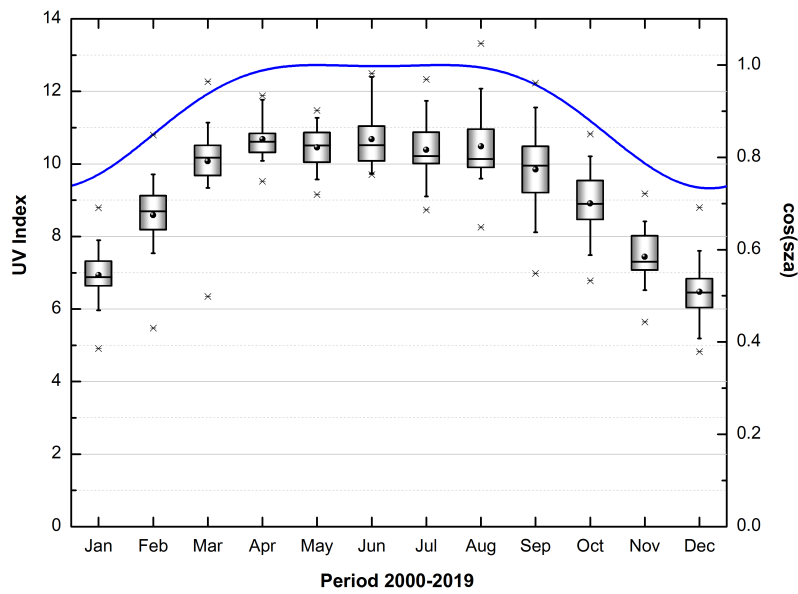


Figure 4: Boxplot of the monthly averages of the maximum UV Index values (black dot) in MCMA for the period 2000-2019: median (central bold line), standard deviation (box edges), 25<sup>th</sup> and 75<sup>th</sup> percentiles (the whiskers), the minimum and maximum values (plus sign) and the cosine of the solar zenith angle at solar noon (blue curve).

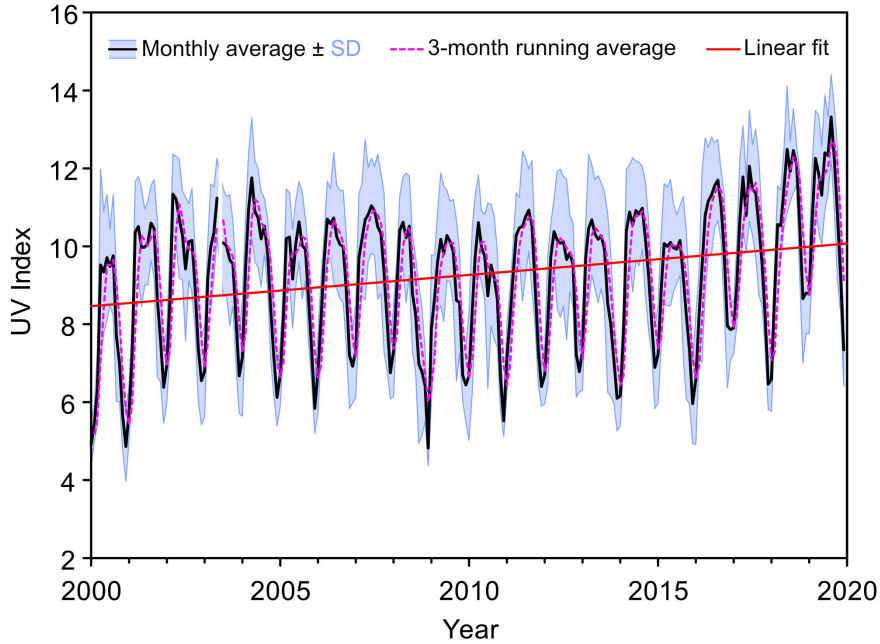


Figure 5: Moving average function (light gray curve) quarterly applied to monthly average UV Index, standard deviation of all data within a given month (black dots and dash line) and linear fit (red line).

201 The UV Index computed from satellite-based observations (OMI-Aura/NIVR-FMI-NASA)

202 over the period 2005-2019 is mapped in Figure 6. The satellite-derived UVIs vary from 8  
 203 in winter to 16 in summer, both values being substantially higher than the ground-based  
 204 observations (ca. 7 for winter and 11 for summer, see Fig. 4). We hypothesize that this large  
 205 difference between satellite-based estimation and ground-based observation of the UV index  
 206 is due to the intense air pollution of Mexico City. A rather similar behavior was detected in  
 207 Santiago city, Chile.<sup>51</sup>

208 Close inspection of Figure 6 shows that the maximum values, those from June and July of  
 209 each year, show a slight but systematic decrease starting ca. 2013. As mentioned in section  
 210 Methods, this is due to the post-processing of OMI UVI data to account for absorption by  
 211 BL aerosols<sup>40</sup>, using a climatological reduction of about 8% for Mexico City.

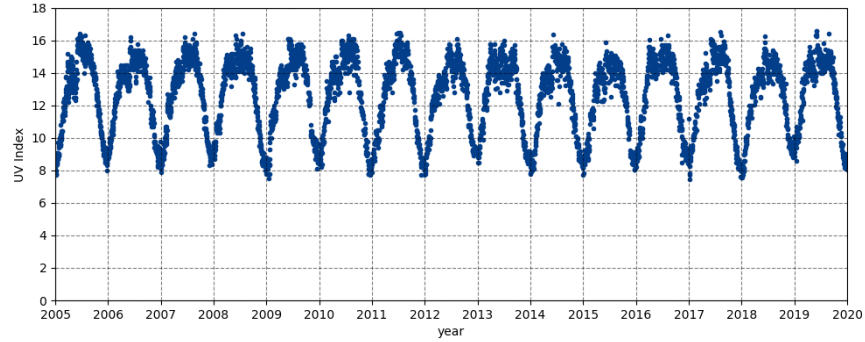


Figure 6: UV Index at solar noon for clear sky recorded by OMI-Aura/NIVR-FMI-NASA, from 2005 to 2019.

## <sup>212</sup> Effect of pollutants on UV radiation

<sup>213</sup> Trends and averages in aerosol optical depth  $AOD_{340}$  and criteria pollutants  $PM_{10}$ , CO,  
<sup>214</sup>  $NO_2$ ,  $O_3$  and  $SO_2$  observed at the SIMAT stations over 2000-2019, are shown in Figure 7  
<sup>215</sup> and summarized in Table 2 together with the  $UVI_{max}$ . Similar trends in pollutants have  
<sup>216</sup> been noted before<sup>52-54</sup> and reflect the long-term success of emission reduction policies and  
<sup>217</sup> programs.

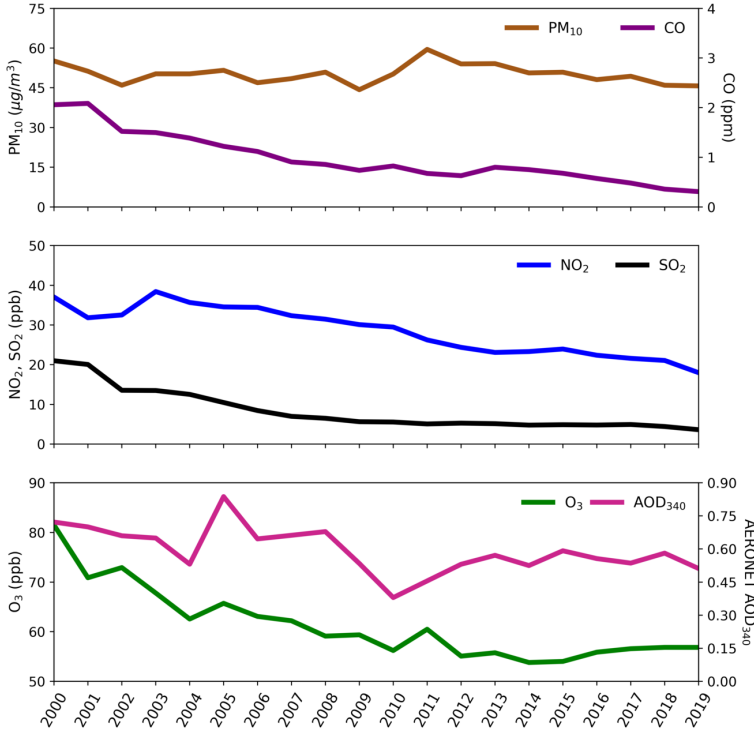


Figure 7: Air quality trends in MCMA for the period 2000-2019 from annual averages obtained between 11h to 15h CST every day: PM<sub>10</sub> (brown curve), CO (purple curve), NO<sub>2</sub> (blue curve), SO<sub>2</sub>(black curve), O<sub>3</sub> (green curve) and AOD<sub>340</sub> (pink curve).

Table 2: UV Index and criteria pollutants: slope for the period 2000-2019, averages in units of  $\mu\text{g}/\text{m}^3$ (PM<sub>10</sub>), ppm (CO), ppb (SO<sub>2</sub>, NO<sub>2</sub> and O<sub>3</sub>), dimensionless (UV Index and AOD<sub>340</sub>) and annual percentage change (%/year).

Variable	$\frac{\Delta \text{variable}}{\Delta t}$	Avg <sub>2000–2019</sub>	$\Delta(\%/\text{year})$
UVI	0.08	9.2	0.9
PM <sub>10</sub>	-0.10	50.2	-0.2
CO	-0.08	1.0	-8.2
NO <sub>2</sub>	-0.96	28.6	-3.4
O <sub>3</sub>	-1.05	61.3	-1.7
AOD <sub>340</sub>	-0.01	0.6	-1.6
SO <sub>2</sub>	-0.76	8.4	-9.1

218     The observed changes in the concentrations of these air pollutants have significant impli-  
 219     cations for surface UV radiation, as can be demonstrated with the TUV radiative transfer  
 220     model. Table 3 summarizes UVI values for the June-July time period, estimated by the

221 three methods: OMI satellite-derived UVI, RAMA ground-based observations, and TUV  
 222 modeling using air pollution estimates. Two groups of values can be readily identified: (1)  
 223 RAMA daily record values, OMI with or without BL aerosols, and TUV for very clean con-  
 224 ditions, all with UVI values around 15-16; and (2) RAMA average daily maxima and TUV  
 225 UVI using MCMA pollutants as input, which are in good agreement for both 2018/19 and  
 226 2000/01 but much lower than the first group. Compared to the OMI estimate that included  
 227 the climatological aerosol correction (15.3), observed RAMA values were lower by 35% in  
 228 2000 and by 20% in 2019. Similarly, TUV values were 35% lower in 2000 and 22% lower in  
 229 2019 relative to the TUV values of 15.6 for a pristine atmosphere.

Table 3: UV Index monthly maximum estimates for June-July.

Conditions for estimation in June-July	UV Index
RAMA maximum reached in period 2000-2019	15.0
RAMA average maxima 2018, 2019	12.3
RAMA average maxima 2000, 2001	9.9
OMI clear, local noon, no corrected for BL aerosols	16.6
OMI with 8% reduction for BL aerosol (Figure 1 from Arola et al.)	15.3
TUV "zero" pollution	16.1
AOD 0, O <sub>3</sub> 0 ppb, NO <sub>2</sub> 0 ppb, SO <sub>2</sub> 0 ppb	
TUV pristine pollution	15.6
AOD 0.05, O <sub>3</sub> 10 ppb, NO <sub>2</sub> 0 ppb, SO <sub>2</sub> 0 ppb	
TUV 2019:	12.1
AOD 0.5, O <sub>3</sub> 50 ppb, NO <sub>2</sub> 20 ppb, SO <sub>2</sub> 1 ppb	
TUV 2000:	10.2
AOD 0.7, O <sub>3</sub> 70 ppb, NO <sub>2</sub> 40 ppb, SO <sub>2</sub> 20 ppb	

230 The agreement between RAMA observations and TUV model estimates is excellent but  
 231 also probably a bit fortuitous. Clouds on average reduce the irradiance impinging on the  
 232 surface, but scattering from them can also cause transient enhancements (especially if the  
 233 direct sunbeam is not blocked) that could be recorded as daily maxima – with cancellation  
 234 between these cloud effects resulting in improved agreement with the cloud-free model. We  
 235 cannot exclude that some of the observed trend in UVI is due to changes in cloud cover.  
 236 However, the modeled fractional UVI reductions due to pollutants, shown in Table 3, are in

<sup>237</sup> such good agreement with the observed UVI reductions, that a compelling case can be made  
<sup>238</sup> for a dominant role of air pollutants in the long-term UVI trends.

<sup>239</sup> Table 4 shows the contributions to UVI reductions from individual pollutants. Aerosols  
<sup>240</sup> are seen to be the major factor in both time periods, followed by O<sub>3</sub>, NO<sub>2</sub>, and SO<sub>2</sub>. The  
<sup>241</sup> 2000-2019 UVI increase is seen to result in comparable proportions from fewer aerosols, less  
<sup>242</sup> SO<sub>2</sub>, and the combined reductions in O<sub>3</sub> and NO<sub>2</sub>.

<sup>243</sup> Comparable UV reductions, of 30-40% due to aerosols, were reported by Panicker et al.<sup>11</sup>  
<sup>244</sup> over Pune, India from April 2004 to March 2005, with sensitivity coefficients (i.e. change in  
<sup>245</sup> UVI per unit change in AOD) similar to those found here in Table 3.

<sup>246</sup> Comparisons of OMI with ground-based UV measurements have been reviewed recently  
<sup>247</sup> by Zhang et al.<sup>55</sup> and Vitt et al.<sup>56</sup>. OMI-derived UV generally overestimates ground-level  
<sup>248</sup> measurements by 1-10% in relatively clean conditions (e.g. rural U.S), by 10-30% in Southern  
<sup>249</sup> Europe and by 40% or more in Santiago, Chile<sup>51</sup> and Thailand<sup>57</sup>. The overestimations appear  
<sup>250</sup> related in large part to incomplete accounting of UV absorption by BL aerosol, although  
<sup>251</sup> other factors such as the correction to solar noon may also introduce some bias.<sup>55</sup> Over  
<sup>252</sup> Europe, ground-based UVI observations for several decades are systematically lower than  
<sup>253</sup> those estimated from satellites even after consideration of climatological aerosol distributions,  
<sup>254</sup> showing the importance of local pollution not resolved from space.<sup>56</sup> However, difference  
<sup>255</sup> between satellite-derived and ground-based UVI was less than 1.0 UVI units in over 90% of  
<sup>256</sup> the cases, in contrast to the difference of 3-5 units found for Mexico City (Table 3).

<sup>257</sup> UV reductions by air pollutants are expected to be most severe near the surface, while  
<sup>258</sup> chemical reactions leading to photochemical smog occur through the vertical extent of the  
<sup>259</sup> BL. Figure 8 shows the vertical profiles of photolysis coefficients (the reciprocals of photolytic  
<sup>260</sup> lifetimes) for two key reactions, the photolysis of O<sub>3</sub> to yield excited oxygen atoms O(1D),  
<sup>261</sup> and the photolysis of NO<sub>2</sub>. In the absence of optically active pollutants, these coefficients  
<sup>262</sup> would be nearly independent of altitude in the BL. However, the presence of pollutants  
<sup>263</sup> leads to a strong decrease toward the surface, with notably more severe reductions in 2000

264 compared to 2019. While the specific values shown in the figure are only illustrative for  
 265 typical conditions, routine daily air quality modeling should carefully account for the long  
 266 term variations in these photolysis coefficients.

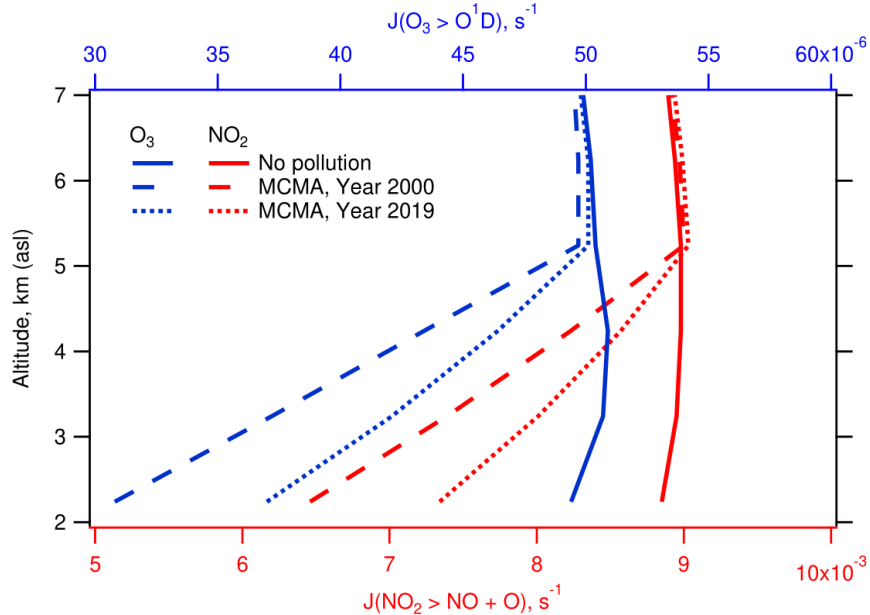


Figure 8: Vertical profiles of the photolysis coefficients for the reaction  $O_3 + h\nu \rightarrow O(1D) + O_2$  (top axis, blue)  $NO_2 + h\nu \rightarrow O + NO$  (bottom axis, red) for zero pollution (solid) and Mexico City in the years 2000 (dashed) and 2019 (dotted)

267 An issue that is beginning to gain relevance in radiative balance models is the influence  
 268 of a group of organic compounds capable of strongly absorbing in the UV region (brown  
 269 carbon).<sup>58</sup> Some of these compounds are related with emissions from local and regional  
 270 wildfires.<sup>59</sup> Mexico City is frequently exposed to regional fire smoke transport during the  
 271 dry part of the year (November to May)<sup>60</sup>, that sporadically modify the optical properties of  
 272 the aerosols.<sup>61</sup> This could partly explain the relatively minor reductions in PM<sub>10</sub> (see Fig. 7),  
 273 compared to the larger reductions of CO, NO<sub>2</sub>, and O<sub>3</sub> that are more directly related to urban  
 274 activities, as well as some of the seasonal asymmetry seen in Fig. 3.

275 The UVI is specific to wavelengths mainly in the 300-320 nm range, and so the question  
 276 remains whether these results can be applied at longer UV wavelengths, e.g. those important  
 277 for NO<sub>2</sub> photolysis (<420 nm). Absorption by SO<sub>2</sub> and O<sub>3</sub> vanishes, while absorption by NO<sub>2</sub>

278 increases and typical aerosols optical depth decrease. These changes can easily be modeled,  
279 but unfortunately far fewer measurements of these longer wavelengths are available in Mexico  
280 City or elsewhere.

281 Two decades of observations in Mexico City demonstrate unequivocally that air pollution  
282 reduces UV radiation at the ground. The ground-based observations are well below estimates  
283 derived from satellite-based observations, and below model calculations do not consider  
284 optically important pollutant aerosols, tropospheric ozone, and to a lesser extent NO<sub>2</sub> and  
285 SO<sub>2</sub>. When typical observed values of these pollutants are included in a model (e.g. TUV),  
286 the differences between satellite-derived and ground-based measured values are explained and  
287 can be attributed quantitatively to individual observed pollutants. Long term improvements  
288 in air quality, over two decades, are accompanied by statistically significant increases in the  
289 observed UVI, again in good agreement with the model-predicted changes.

Table 4: Contributions of individual pollutants to UV Index changes. (a) Values used one at the time, with the others held at zero. (b) UVI deviation from the zero-pollution value of 16.1 (from Table 3). (c) 2019-2000 UVI change due to changes in each pollutant.

Pollutant	Year 2000		Year 2019		2019-2000
	poll. level (a)	UVI (b)	poll. level	UVI	(c)
AOD	0.7	-3.7	0.5	-2.7	1.0
O <sub>3</sub> ppb (DU)	70 (14)	-1.4	50 (10)	-1.0	0.4
NO <sub>2</sub> ppb	40	-0.9	20	-0.5	0.4
SO <sub>2</sub> ppb	30	-0.8	1	-0.04	0.8

290 The reductions in surface UV radiation with respect to an ideally clear atmosphere –  
291 by nearly 40% in 2000 and still 20% in 2020 – are large, both within the context of hu-  
292 man UV exposure and air quality mitigation. In urban areas where ozone production scales  
293 proportionally with UV levels and with volatile organic compound (VOC) emissions (the  
294 VOC-limited regime), a 10% increase in BL average photolysis rates means that VOC emis-  
295 sions will need to be reduced by 10% to meet the same goals, or else successful reductions in  
296 aerosols would lead to unwanted UV-driven increases in O<sub>3</sub>. Such UV changes must be con-  
297 sidered carefully in air quality mitigation strategies. For human exposure, a 20% increase in

298 UV irradiances over two decades should be seen as a non-negligible public health issue requiring  
299 some reassessment of preventive behaviors to minimize the risk of skin cancer, cataract,  
300 and other UV-related health effects. The efforts that Mexico City has made to improve air  
301 quality have achieved positive results in the levels of most air pollutants. Nevertheless, they  
302 caused an increase in UV radiation that reaches the surface.

303 A limitation of the present work is our focus on daily maximum values, which largely  
304 exclude cloud cover. Absorption within clouds can be enhanced by the long path lengths  
305 of multiply scattered photons (e.g., Mayer et al.<sup>62</sup>), so that accurate quantification of UV  
306 effects of clouds in polluted environments remains a significant challenge and interesting  
307 opportunity for future work.

308 Finally, based on our results, the solar radiation monitoring network could be improved  
309 by adding observation sites within or close to the basin, with minor influences of the urban  
310 plume (e. g., Amecameca; latitude: 19.13°N, longitude: 99.76°W, elevation: 2420 m asl),  
311 and the complementing of sensors in existing monitoring sites that are at elevations above the  
312 urban boundary layer like Ajusco (AJU, elevation: 2953 m asl) or Instituto de Investigaciones  
313 Nucleares (INN, elevation: 3082 m asl). These sites would provide valuable observations to  
314 assess quantitatively the effects of urban pollution on solar radiation levels.

## 315 Acknowledgement

316 We wish to acknowledge the staff of SIMAT, from the Secretariat of Environment, for the  
317 data and the continuous assistance during the realization of this project. Adriana Ipiña would  
318 like to extend her thanks to Dirección General de Personal Académico, Universidad Nacional  
319 Autónoma de México (DGAPA-UNAM) for the postdoctoral fellowship at Centro de Ciencias  
320 de la Atmósfera of the UNAM. Rubén D Piacentini wishes to thank CONICET and National  
321 University of Rosario, Argentina, for their partial support to the present work. The National  
322 Center for Atmospheric Research is sponsored by the National Science Foundation.

323 **References**

- 324 (1) Taylor, H. R.; West, S. K.; Rosenthal, F. S.; Muñoz, B.; Newland, H. S.; Abbey, H.;  
325 Emmett, E. A. Effect of Ultraviolet Radiation on Cataract Formation. *New England  
326 Journal of Medicine* **1988**, *319*, 1429–1433.
- 327 (2) Varotsos, C.; Feretis, E. Health effects on human eye resulting from the increased  
328 ambient solar ultraviolet radiation. *Toxicological & Environmental Chemistry* **1997**,  
329 *61*, 43–68.
- 330 (3) Lucas, R. M.; Yazar, S.; Young, A. R.; Norval, M.; de Gruijl, F. R.; Takizawa, Y.;  
331 Rhodes, L. E.; Sinclair, C. A.; Neale, R. E. Human health in relation to exposure to solar  
332 ultraviolet radiation under changing stratospheric ozone and climate. *Photochemical &  
333 Photobiological Sciences* **2019**, *18*, 641–680.
- 334 (4) Leighton, P. A. *Photochemistry of Air Pollution*; Elsevier, 1961; pp v–vi.
- 335 (5) Seinfeld, J. H.; Pandis, S. N.; Noone, K. Atmospheric Chemistry and Physics: From  
336 Air Pollution to Climate Change. *Physics Today* **1998**, *51*, 88–90.
- 337 (6) Finlayson-Pitts, B. J.; Pitts, J. N. *Chemistry of the Upper and Lower Atmosphere*;  
338 Academic Press, 2000; pp xvii–xviii.
- 339 (7) Liu, S. C.; McKeen, S. A.; Madronich, S. Effect of anthropogenic aerosols on biologically  
340 active ultraviolet radiation. *Geophysical Research Letters* **1991**, *18*, 2265–2268.
- 341 (8) Sabziparvar, A. A.; Forster, P. M. F.; Shine, K. P. Changes in ultraviolet radiation due  
342 to stratospheric and tropospheric ozone changes since preindustrial times. *Journal of  
343 Geophysical Research: Atmospheres* **1998**, *103*, 26107–26113.
- 344 (9) Madronich, S.; Wagner, M.; Groth, P. Influence of Tropospheric Ozone Control on  
345 Exposure to Ultraviolet Radiation at the Surface. *Environmental Science & Technology*  
346 **2011**, *45*, 6919–6923.

- 347 (10) McKenzie, R. L.; Weinreis, C.; Johnston, P. V.; Liley, B.; Shiona, H.; Kotkamp, M.;  
348 Smale, D.; Takegawa, N.; Kondo, Y. Effects of urban pollution on UV spectral irradi-  
349 ances. *Atmospheric Chemistry and Physics* **2008**, *8*, 5683–5697.
- 350 (11) Panicker, A. S.; Pandithurai, G.; Takamura, T.; Pinker, R. T. Aerosol effects in the  
351 UV-B spectral region over Pune an urban site in India. *Geophysical Research Letters*  
352 **2009**, *36*, L10802 1–5.
- 353 (12) Palancar, G. G.; Lefer, B. L.; Hall, S. R.; Shaw, W. J.; Corr, C. A.; Herndon, S. C.;  
354 Slusser, J. R.; Madronich, S. Effect of aerosols and NO<sub>2</sub> concentration on ultraviolet  
355 actinic flux near Mexico City during MILAGRO: measurements and model calculations.  
356 *Atmospheric Chemistry and Physics* **2013**, *13*, 1011–1022.
- 357 (13) Bais, A. F.; McKenzie, R. L.; Bernhard, G.; Aucamp, P. J.; Ilyas, M.; Madronich, S.;  
358 Tourpali, K. Ozone depletion and climate change: impacts on UV radiation. *Photo-  
359 chemical & Photobiological Sciences* **2015**, *14*, 19–52.
- 360 (14) Hollaway, M.; Wild, O.; Yang, T.; Sun, Y.; Xu, W.; Xie, C.; Whalley, L.; Slater, E.;  
361 Heard, D.; Liu, D. Photochemical impacts of haze pollution in an urban environment.  
362 *Atmospheric Chemistry and Physics* **2019**, *19*, 9699–9714.
- 363 (15) Li, K.; Jacob, D. J.; Liao, H.; Shen, L.; Zhang, Q.; Bates, K. H. Anthropogenic drivers  
364 of 2013–2017 trends in summer surface ozone in China. *Proceedings of the National  
365 Academy of Sciences* **2018**, *116*, 422–427.
- 366 (16) Wang, Y. et al. *Contrasting trends of PM2.5 and surface-ozone concentrations in China  
367 from 2013 to 2017*; Oxford University Press (OUP), 2020; Vol. 7; pp 1331–1339.
- 368 (17) Wang, W.; Li, X.; Shao, M.; Hu, M.; Zeng, L.; Wu, Y.; Tan, T. The impact of aerosols  
369 on photolysis frequencies and ozone production in Beijing during the 4-year period  
370 2012–2015. *Atmospheric Chemistry and Physics* **2019**, *19*, 9413–9429.

- 371 (18) Gao, J.; Li, Y.; Zhu, B.; Hu, B.; Wang, L.; Bao, F. What have we missed when studying  
372 the impact of aerosols on surface ozone via changing photolysis rates? *Atmospheric*  
373 *Chemistry and Physics* **2020**, *20*, 10831–10844.
- 374 (19) Bauwens, M.; Compernolle, S.; Stavrakou, T.; Müller, J.-F.; Gent, J.; Eskes, H.; Lev-  
375 elt, P. F.; A, R.; Veefkind, J. P.; Vlietinck, J.; Yu, H.; Zehner, C. Impact of coronavirus  
376 outbreak on NO<sub>2</sub> pollution assessed using TROPOMI and OMI observations. **2020**,  
377 *47*, e2020GL087978.
- 378 (20) Venter, Z. S.; Aunan, K.; Chowdhury, S.; Lelieveld, J. COVID-19 lockdowns cause  
379 global air pollution declines. *Proceedings of the National Academy of Sciences* **2020**,  
380 *117*, 18984–18990.
- 381 (21) Shi, X.; Brasseur, G. P. The Response in Air Quality to the Reduction of Chinese  
382 Economic Activities During the COVID-19 Outbreak. *Geophysical Research Letters*  
383 **2020**, *47*, e2020GL088070.
- 384 (22) Le, T.; Wang, Y.; Liu, L.; Yang, J.; Yung, Y. L.; Li, G.; Seinfeld, J. H. Unexpected air  
385 pollution with marked emission reductions during the COVID-19 outbreak in China.  
386 *Science* **2020**, *369*, 702–706.
- 387 (23) Red Automática de Monitoreo Atmosférico (RAMA). <http://www.aire.cdmx.gob.mx/descargas/datos/excel/RAMA.xls.pdf>.
- 388 (24) Doran, J. C. et al. The IMADA-AVER Boundary Layer Experiment in the Mexico City  
389 Area. *Bulletin of the American Meteorological Society* **1998**, *79*, 2497–2508.
- 390 (25) Molina, L. T.; Kolb, C. E.; de Foy, B.; Lamb, B. K.; Brune, W. H.; Jimenez, J. L.;  
391 Ramos-Villegas, R.; Sarmiento, J.; Paramo-Figueroa, V. H.; Cardenas, B.; Gutierrez-  
392 Avedoy, V.; Molina, M. J. Air quality in North America's most populous city – overview  
393 of the MCMA-2003 campaign. *Atmospheric Chemistry and Physics* **2007**, *7*, 2447–2473.

- 395 (26) Molina, L. T. et al. An overview of the MILAGRO 2006 Campaign: Mexico City  
396 emissions and their transport and transformation. *Atmospheric Chemistry and Physics*  
397 **2010**, *10*, 8697–8760.
- 398 (27) Jazcilevich, A. D.; García, A. R.; Caetano, E. Locally induced surface air confluence  
399 by complex terrain and its effects on air pollution in the valley of Mexico. *Atmospheric*  
400 *Environment* **2005**, *39*, 5481–5489.
- 401 (28) Tie, X.; Madronich, S.; Li, G.; Ying, Z.; Zhang, R.; Garcia, A. R.; Lee-Taylor, J.; Liu, Y.  
402 Characterizations of chemical oxidants in Mexico City: A regional chemical dynamical  
403 model (WRF-Chem) study. *Atmospheric Environment* **2007**, *41*, 1989–2008.
- 404 (29) Zhang, Y.; Dubey, M. K.; Olsen, S. C.; Zheng, J.; Zhang, R. Comparisons of  
405 WRF/Chem simulations in Mexico City with ground-based RAMA measurements dur-  
406 ing the 2006-MILAGRO. *Atmospheric Chemistry and Physics* **2009**, *9*, 3777–3798.
- 407 (30) Zavala, M.; Brune, W. H.; Velasco, E.; Retama, A.; Cruz-Alavez, L. A.; Molina, L. T.  
408 Changes in ozone production and VOC reactivity in the atmosphere of the Mexico City  
409 Metropolitan Area. *Atmospheric Environment* **2020**, *238*, 117747.
- 410 (31) WHO,; WMO,; UNEP,; ICNIRP, *Global solar UV index : a practical guide*; 2002; pp A  
411 joint recommendation of the World Health Organization, World Meteorological Orga-  
412 nization, United Nations Environment Programme, and the International Commission  
413 on Non-Ionizing Radiation Protection.
- 414 (32) Webb, A. R.; Slaper, H.; Koepke, P.; Schmalwieser, A. W. Know Your Standard: Clari-  
415 fying the CIE Erythema Action Spectrum. *Photochemistry and Photobiology* **2011**, *87*,  
416 483–486.
- 417 (33) Whiteman, C. D.; Zhong, S.; Bian, X.; Fast, J. D.; Doran, J. C. Boundary layer evo-  
418 lution and regional-scale diurnal circulations over the Mexican plateau. *Journal of*  
419 *Geophysical Research: Atmospheres* **2000**, *105*, 10081–10102.

- 420 (34) Fast, J. D.; de Foy, B.; Rosas, F. A.; Caetano, E.; Carmichael, G.; Emmons, L.;  
421 McKenna, D.; Mena, M.; Skamarock, W.; Tie, X.; Coulter, R. L.; Barnard, J. C.;  
422 Wiedinmyer, C.; Madronich, S. A meteorological overview of the MILAGRO field cam-  
423 paigns. *Atmospheric Chemistry and Physics* **2007**, *7*, 2233–2257.
- 424 (35) Carreón-Sierra, S.; Salcido, A.; Castro, T.; Celada-Murillo, A.-T. Cluster Analysis of  
425 the Wind Events and Seasonal Wind Circulation Patterns in the Mexico City Region.  
426 *Atmosphere* **2015**, *6*, 1006–1031.
- 427 (36) Sistema de Monitoreo Atmosférico (SIMAT). [www.aire.cdmx.gob.mx](http://www.aire.cdmx.gob.mx), [www.aire.cdmx.gob.mx/default.php](http://www.aire.cdmx.gob.mx/default.php).
- 428
- 429 (37) Holben, B.; Eck, T.; Slutsker, I.; Tanré, D.; Buis, J.; Setzer, A.; Vermote, E.; Reagan, J.;  
430 Kaufman, Y.; Nakajima, T.; Lavenu, F.; Jankowiak, I.; Smirnov, A. AERONET—A  
431 Federated Instrument Network and Data Archive for Aerosol Characterization. *Remote  
432 Sensing of Environment* **1998**, *66*, 1–16.
- 433 (38) Carabali, G.; Estévez, H. R.; Valdés-Barrón, M.; Bonifaz-Alfonzo, R.; Riveros-  
434 Rosas, D.; Velasco-Herrera, V. M.; Vázquez-Gálvez, F. A. Aerosol climatology over  
435 the Mexico City basin: Characterization of optical properties. *Atmospheric Research*  
436 **2017**, *194*, 190–201.
- 437 (39) NASA EOS/Aura Validation Data Center (AVDC) - Correlative data, Field of  
438 View Predictions, Data Subsets, GEOMS, DCIO. [https://avdc.gsfc.nasa.gov/pub/  
439 most\\_popular/overpass/OMI/](https://avdc.gsfc.nasa.gov/pub/most_popular/overpass/OMI/).
- 440 (40) Arola, A. et al. A new approach to correct for absorbing aerosols in OMI UV. *Geophys-  
441 ical Research Letters* **2009**, *36*, L22805 1–5.
- 442 (41) Madronich, S. Intercomparison of NO<sub>2</sub> photodissociation and U.V. Radiometer Mea-  
443 surements. *Atmospheric Environment* **1987**, *21*, 569–578.

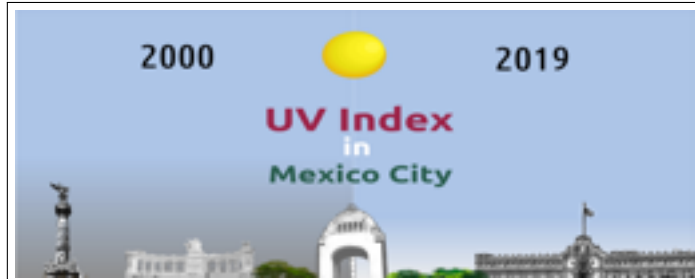
- 444 (42) Shaw, W. J.; Pekour, M. S.; Coulter, R. L.; Martin, T. J.; Walters, J. T. The daytime  
445 mixing layer observed by radiosonde profiler, and lidar during MILAGRO. *Atmospheric*  
446 *Chemistry and Physics Discussions* **2007**, *7*, 15025–15065.
- 447 (43) Velasco, E.; Márquez, C.; Bueno, E.; Bernabé, R. M.; Sánchez, A.; Fentanes, O.; Wöhrn-  
448 schimmel, H.; Cárdenas, B.; Kamilla, A.; Wakamatsu, S.; Molina, L. T. Vertical dis-  
449 tribution of ozone and VOCs in the low boundary layer of Mexico City. *Atmospheric*  
450 *Chemistry and Physics* **2008**, *8*, 3061–3079.
- 451 (44) Greenberg, J.; Guenther, A.; Turnipseed, A. Tethered balloon-based soundings of ozone  
452 aerosols, and solar radiation near Mexico City during MIRAGE-MEX. *Atmospheric*  
453 *Environment* **2009**, *43*, 2672–2677.
- 454 (45) Rogers, R. R.; Hair, J. W.; Hostetler, C. A.; Ferrare, R. A.; Obland, M. D.; Cook, A. L.;  
455 Harper, D. B.; Burton, S. P.; Shinozuka, Y.; McNaughton, C. S.; Clarke, A. D.; Re-  
456 demann, J.; Russell, P. B.; Livingston, J. M.; Kleinman, L. I. NASA LaRC airborne  
457 high spectral resolution lidar aerosol measurements during MILAGRO: observations  
458 and validation. *Atmospheric Chemistry and Physics* **2009**, *9*, 4811–4826.
- 459 (46) Lewandowski, P. A.; Eichinger, W. E.; Holder, H.; Prueger, J.; Wang, J.; Kleinman, L. I.  
460 Vertical distribution of aerosols in the vicinity of Mexico City during MILAGRO-2006  
461 Campaign. *Atmospheric Chemistry and Physics* **2010**, *10*, 1017–1030.
- 462 (47) Corr, C. A.; Krotkov, N.; Madronich, S.; Slusser, J. R.; Holben, B.; Gao, W.; Flynn, J.;  
463 Lefer, B.; Kreidenweis, S. M. Retrieval of aerosol single scattering albedo at ultraviolet  
464 wavelengths at the T1 site during MILAGRO. *Atmospheric Chemistry and Physics*  
465 **2009**, *9*, 5813–5827.
- 466 (48) Castro, T.; Madronich, S.; Rivale, S.; Muhlia, A.; Mar, B. The influence of aerosols on  
467 photochemical smog in Mexico City. *Atmospheric Environment* **2001**, *35*, 1765–1772.
- 468 (49) SEDEMA, *Calidad del aire en la Ciudad de México, Informe 2017*; 2018.

- 469 (50) Retama, A.; Baumgardner, D.; Raga, G. B.; McMeeking, G. R.; Walker, J. W. Sea-  
470       sonal and diurnal trends in black carbon properties and co-pollutants in Mexico City.  
471       *Atmospheric Chemistry and Physics* **2015**, *15*, 9693–9709.
- 472 (51) Cabrera, S.; Ipiña, A.; Damiani, A.; Cordero, R. R.; Piacentini, R. D. UV index values  
473       and trends in Santiago Chile ( $33.5^{\circ}\text{S}$ ) based on ground and satellite data. *Journal of*  
474       *Photochemistry and Photobiology B: Biology* **2012**, *115*, 73–84.
- 475 (52) Parrish, D. D.; Singh, H. B.; Molina, L.; Madronich, S. Air quality progress in North  
476       American megacities: A review. *Atmospheric Environment* **2011**, *45*, 7015–7025.
- 477 (53) Secretaría del Medio Ambiente de la Ciudad de México, *Calidad del aire en la Ciudad*  
478       *de México, informe 2017; 2018*; pp 1–160.
- 479 (54) Molina,; Velasco,; Retama,; Zavala, Experience from Integrated Air Quality Manage-  
480       ment in the Mexico City Metropolitan Area and Singapore. *Atmosphere* **2019**, *10*,  
481       512.
- 482 (55) Zhang, H.; Wang, J.; García, L. C.; Zeng, J.; Dennhardt, C.; Liu, Y.; Krotkov, N. A.  
483       Surface erythemal UV irradiance in the continental United States derived from ground-  
484       based and OMI observations: quality assessment trend analysis and sampling issues.  
485       *Atmospheric Chemistry and Physics* **2019**, *19*, 2165–2181.
- 486 (56) Vitt, R.; Laschewski, G.; Bais, A.; Diémoz, H.; Fountoulakis, I.; Siani, A.-M.;  
487       Matzarakis, A. UV-Index Climatology for Europe Based on Satellite Data. *Atmosphere*  
488       **2020**, *11*, 727.
- 489 (57) Janjai, S.; Wisitsirikun, S.; Buntoung, S.; Pattarapanitchai, S.; Wattan, R.; Masiri, I.;  
490       Bhattarai, B. K. Comparison of UV index from Ozone Monitoring Instrument (OMI)  
491       with multi-channel filter radiometers at four sites in the tropics: effects of aerosols and  
492       clouds. *International Journal of Climatology* **2013**, *34*, 453–461.

- 493 (58) Laskin, A.; Laskin, J.; Nizkorodov, S. A. Chemistry of Atmospheric Brown Carbon.
- 494       *Chemical Reviews* **2015**, *115*, 4335–4382.
- 495 (59) Gadhavi, H.; Jayaraman, A. Absorbing aerosols: contribution of biomass burning and
- 496       implications for radiative forcing. *Annales Geophysicae* **2010**, *28*, 103–111.
- 497 (60) Rios, B.; Raga, G. B. Smoke emissions from agricultural fires in Mexico and Central
- 498       America. *Journal of Applied Remote Sensing* **2019**, *13*, 1.
- 499 (61) Barnard, J. C.; Volkamer, R.; Kassianov, E. I. Estimation of the mass absorption cross
- 500       section of the organic carbon component of aerosols in the Mexico City Metropolitan
- 501       Area. *Atmospheric Chemistry and Physics* **2008**, *8*, 6665–6679.
- 502 (62) Mayer, B.; Kylling, A.; Madronich, S.; Seckmeyer, G. Enhanced absorption of UV
- 503       radiation due to multiple scattering in clouds: Experimental evidence and theoretical
- 504       explanation. *Journal of Geophysical Research: Atmospheres* **1998**, *103*, 31241–31254.

505 Graphical TOC Entry

506



Some journals require a graphical entry for the Table of Contents. This should be laid out “print ready” so that the sizing of the text is correct.

Inside the `tocentry` environment, the font used is Helvetica 8 pt, as required by *Journal of the American Chemical Society*.

The surrounding frame is 9 cm by 3.5 cm, which is the maximum permitted for *Journal of the American Chemical Society* graphical table of content entries. The box will not resize if the content is too big: instead it will overflow the edge of the box.

This box and the associated title will always be printed on a separate page at the end of the document.